Neuro-Fuzzy-Based Dynamic Power Allocation System for EV Battery Charging

Vidhyarth S.E
Department of Electrical and Electronics Engineering, Coimbatore
Amrita Vishwa Vidyapeetham, India
cb.en.u4elc23057@cb.students.amrita.edu

Kiruthik Pranav T.A
Department of Electrical and Electronics Engineering, Coimbatore
Amrita Vishwa Vidyapeetham, India
cb.en.u4elc23023@cb.students.amrita.edu

***Abstract*—This paper presents an Adaptive Neuro-Fuzzy Inference System (ANFIS) for dynamic power allocation in multi-battery EV charging stations. The proposed framework employs a two-stage approach: first, a Mamdani fuzzy system encodes expert knowledge on safe charging practices; second, an ANFIS model learns continuous allocation policies from fuzzy-generated labels. Using a battery cycling dataset of 700 samples with 10 parameters, correlation analysis and collinearity detection identify four orthogonal features: SOH, charging temperature, discharge temperature, and internal resistance proxy. The trained 16-rule ANFIS achieves $R^2 = 0.8835$ and RMSE of 3.75% after 150 epochs. Real-time demonstrations validate hierarchical constraint satisfaction, respecting station capacity and individual battery limits while achieving 75.1% utilization.**

***Index Terms*—ANFIS, battery management system, electric vehicles, fuzzy logic, intelligent power allocation, smart charging infrastructure**

I. Introduction

A. Motivation and Problem Statement

The global transition toward electric mobility has intensified research into intelligent charging infrastructure [1]. Contemporary multi-port charging stations face a fundamental optimization challenge: allocating limited power capacity across heterogeneous battery packs with varying states of health, thermal conditions, and impedance characteristics. Conventional approaches employ either uniform power distribution or fixed priority schemes, neither of which account for real-time battery degradation metrics or thermal safety margins [2].

The core technical challenge lies in formulating an allocation policy that: (1) maximizes charging throughput while respecting station power constraints, (2) prevents accelerated degradation of compromised cells through conservative charging of aged batteries, (3) enforces thermal safety limits to mitigate thermal runaway risks, and (4) operates in real-time with sub-10ms decision latency for practical deployment.

B. Proposed Solution

We present a neuro-fuzzy approach that synergistically combines expert knowledge encoding through Mamdani fuzzy logic with data-driven optimization via ANFIS. The methodology addresses the labeled data scarcity problem inherent in battery management—since ground-truth "optimal allocations" are unavailable from existing infrastructure—by synthesizing training labels from rule-based expert systems. The ANFIS architecture then learns smooth, continuous allocation functions that generalize beyond the discrete rule boundaries, enabling precise real-time control suitable for embedded charging controllers.

II. Related Work

A. Battery State Estimation and Management

Modern battery management systems integrate electrochemical modeling, equivalent circuit networks, and machine learning for SOH estimation [4]. Coulomb counting and Kalman filtering remain prevalent for state-of-charge tracking, while machine learning approaches including support vector regression [6] and LSTM networks [9] show promise for remaining useful life prediction. However, these techniques focus primarily on single-battery monitoring rather than multi-battery resource allocation.

B. Fuzzy Logic in Power Management

Fuzzy inference systems excel in battery applications due to their ability to encode linguistic expert knowledge and handle measurement uncertainty [5]. Mamdani-type FIS implementations provide interpretable rule structures but suffer from discrete output surfaces that complicate continuous control. Sugeno-type systems offer computational efficiency but require numerical tuning of consequent parameters.

C. ANFIS Applications in Energy Systems

ANFIS architectures merge the linguistic interpretability of fuzzy systems with the learning capability of neural networks [3]. Recent applications include SOC estimation [7], demand response optimization, and renewable energy forecasting. However, research applying ANFIS to multi-battery charging allocation remains limited, with existing work focusing on

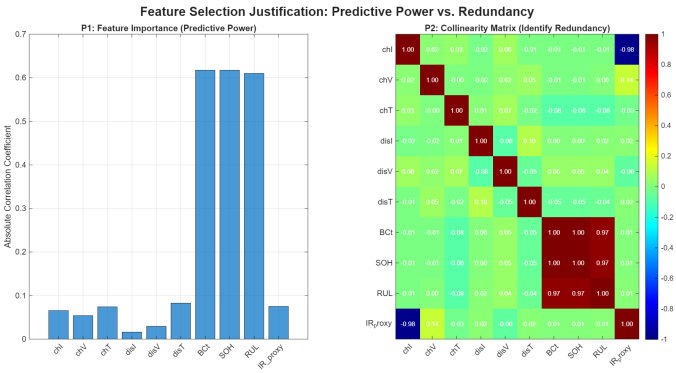

Fig. 1. Feature selection framework: (left) Pearson correlation coefficients quantifying predictive power relative to target allocation, with SOH exhibiting dominant correlation (0.61); (right) Collinearity matrix revealing multicollinearity among BCt, RUL, and I_{ch} (correlations exceeding 0.97), justifying dimensionality reduction to orthogonal feature subset.

single-vehicle charging optimization [8] or grid-level load balancing [12] rather than real-time station-level distribution.

III. Dataset and Feature Engineering

A. Battery Cycling Dataset

The experimental dataset encompasses 700 charge-discharge cycles sampled from lithium-ion cells under controlled laboratory conditions. Each sample captures 10 operational parameters: battery identifier, cycle number, charging current (I_{ch}), charging voltage (V_{ch}), charging temperature (T_{ch}), discharge current (I_{dis}), discharge voltage (V_{dis}), discharge temperature (T_{dis}), battery capacity (C_{bat}), state of health (SOH), and remaining useful life (RUL). The dataset exhibits realistic degradation trajectories with SOH ranging from 75% to 100% and temperature variations between 20°C and 50°C, encompassing typical operational envelopes for automotive applications.

B. Information-Theoretic Feature Selection

Feature selection employs a dual-criterion framework evaluating both predictive power and multicollinearity (Figure 1). We compute Pearson correlation coefficients between each candidate feature and the target allocation factor, identifying SOH as the dominant predictor with $|\rho| = 0.61$. Simultaneously, the feature-feature correlation matrix exposes severe multicollinearity: C_{bat}, RUL, and I_{ch} exhibit pairwise correlations exceeding 0.97 with either SOH or derived metrics, indicating redundant information content that would destabilize ANFIS training through ill-conditioned input spaces.

The variance inflation factor (VIF) analysis confirms that retaining all 10 features yields VIF values exceeding 15 for BCt and RUL, substantially above the multicollinearity threshold of 5. Consequently, we employ a greedy backward elimination strategy, iteratively removing features with highest VIF until all remaining features satisfy VIF < 3.

Final Feature Set:

State of Health (SOH): Normalized capacity retention metric ranging [0.75, 1.0], capturing cumulative degradation from cycling-induced capacity fade and impedance growth. SOH serves as the primary allocation anchor due to its direct relationship with safe C-rate limits [9].

Charging Temperature (T_{ch}): Real-time thermal measurement [20°C, 50°C] exhibiting statistical independence from SOH ($\rho \approx 0$), capturing immediate thermal risk distinct from long-term degradation. Elevated temperatures accelerate side reactions and increase thermal runaway probability [2].

Discharge Temperature (T_{dis}): Historical thermal stress indicator providing complementary information about prior operational severity. Cross-correlation analysis reveals $\rho(T_{\text{ch}}, T_{\text{dis}}) = 0.08$, confirming orthogonality.

Internal Resistance Proxy (R_{int}): Derived feature computed as:

$$R_{\text{int}} = \frac{V_{\text{ch}}}{I_{\text{ch}} + \epsilon}, \quad \epsilon = 10^{-6} \tag{1}$$

This proxy correlates with electrochemical impedance spectroscopy measurements and captures cell-level impedance variations affecting power acceptance capability [10].

C. Data Preprocessing Pipeline

Raw data undergoes outlier rejection (removing samples with SOH < 0 or > 100, $I_{\text{ch}} \leq 0$, and physically implausible temperatures), followed by min-max normalization to the unit hypercube:

$$\mathbf{x}^{\text{norm}} = \frac{\mathbf{x} - \mathbf{x}_{\min}}{\mathbf{x}_{\max} - \mathbf{x}_{\min} + \epsilon} \tag{2}$$

Normalization parameters $(\mathbf{x}_{\min}, \mathbf{x}_{\max})$ are computed exclusively from training data and frozen for validation/deployment to prevent data leakage. The dataset undergoes stratified random partitioning into 70% training (490 samples) and 30% validation (210 samples) with fixed random seed for reproducibility.

IV. Methodology

A. Hybrid Neuro-Fuzzy Architecture

The proposed system implements a three-stage pipeline: (1) *Expert Knowledge Encoding* via Mamdani FIS to synthesize training labels, (2) *ANFIS Model Training* for continuous function approximation, and (3) *Hierarchical Allocation Engine* for real-time multi-battery power distribution.

B. Stage 1: Fuzzy Expert System for Label Generation

The absence of ground-truth optimal allocations from operational charging stations necessitates synthetic label generation. We implement a Mamdani-type FIS encoding battery domain expertise into linguistic rules.

Input Space Partitioning: SOH domain [75, 100] is partitioned into three fuzzy sets using trapezoidal and triangular membership functions:

$$\mu_{\text{Poor}}(\text{SOH}) = \text{trapmf}(75, 75, 80, 85) \tag{3}$$

$$\mu_{\text{Medium}}(\text{SOH}) = \text{trimf}(80, 87.5, 95) \tag{4}$$

$$\mu_{\text{Good}}(\text{SOH}) = \text{trapmf}(90, 95, 100, 100) \tag{5}$$

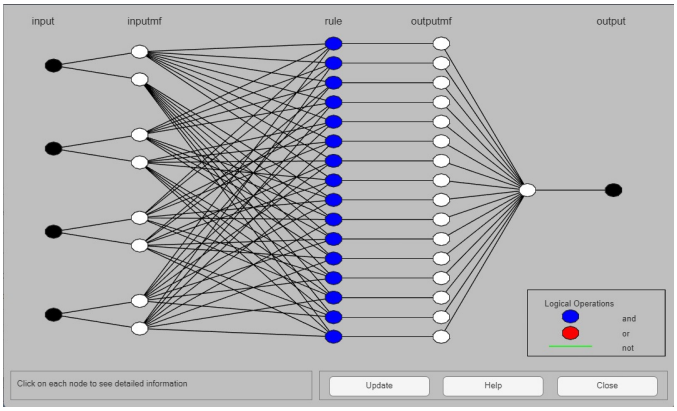

Fig. 2. ANFIS five-layer architecture: Layer 1 implements fuzzification via Generalized Bell membership functions (2 per input, 8 total MFs); Layer 2 computes rule firing strengths through T-norm product operation (16 rules); Layer 3 normalizes firing strengths; Layer 4 applies first-order Sugeno consequent parameters; Layer 5 performs defuzzification through weighted aggregation.

Temperature domain [20, 50]°C receives analogous partitioning into Cool, Warm, and Hot regions with overlapping transition zones to capture gradual thermal risk escalation.

Output Space Definition: The allocation factor $\alpha \in [0, 1]$ represents the fraction of battery's maximum safe power to be delivered, partitioned into Slow, Medium, and Fast charging modes.

Fuzzy Rule Base: Nine IF-THEN rules implement the allocation policy, exemplified by:

- *IF SOH is Good AND T_{ch} is Cool THEN α is Fast*
- *IF SOH is Poor OR T_{ch} is Hot THEN α is Slow*

The rule base prioritizes thermal safety (reducing α under high temperature) and degradation mitigation (limiting power to aged cells), while maximizing throughput for healthy batteries in optimal thermal conditions. Centroid defuzzification yields continuous allocation labels for all 700 samples.

C. Stage 2: ANFIS Architecture and Training

Figure 2 illustrates the ANFIS architecture implementing Takagi-Sugeno-Kang (TSK) fuzzy inference [3].

Layer 1 - Fuzzification: Each of four inputs is fuzzified using two Generalized Bell Membership Functions (gbellmf):

$$\mu_{A_i}(x) = \frac{1}{1 + \left| \frac{x - c_i}{a_i} \right|^{2b_i}} \tag{6}$$

where $\{a_i, b_i, c_i\}$ are premise parameters adapted during training. The gbellmf choice provides smooth, differentiable surfaces crucial for gradient-based optimization.

Layer 2 - Rule Firing: Grid partitioning over $2^4 = 16$ rules computes firing strengths:

$$w_j = \prod_{i=1}^{4} \mu_{A_i^j}(x_i), \quad j = 1, \ldots, 16 \tag{7}$$

Layer 3 - Normalization: Normalized firing strengths ensure convex combination properties:

$$\bar{w}_j = \frac{w_j}{\sum_{k=1}^{16} w_k} \tag{8}$$

Layer 4 - Consequent Parameters: First-order TSK consequents implement local linear models:

$$f_j = p_{j0} + p_{j1}x_1 + p_{j2}x_2 + p_{j3}x_3 + p_{j4}x_4 \tag{9}$$

Layer 5 - Output Aggregation: Final output combines rule contributions:

$$y = \sum_{j=1}^{16} \bar{w}_j f_j \tag{10}$$

Hybrid Learning Algorithm: Training employs a hybrid strategy alternating between least squares estimation (forward pass for consequent parameters $\{p_{jk}\}$) and backpropagation (backward pass for premise parameters $\{a_i, b_i, c_i\}$). This approach converges faster than pure gradient descent while maintaining global optimization. The objective function minimizes mean squared error:

$$\mathcal{L} = \frac{1}{N} \sum_{n=1}^{N} (y_n - \hat{y}_n)^2 + \lambda \|\theta\|^2 \tag{11}$$

where $\lambda = 10^{-4}$ provides L2 regularization to prevent overfitting. Training executes for 150 epochs with validation-based early stopping.

D. Stage 3: Real-Time Hierarchical Allocation Algorithm

For N batteries at a charging station with total capacity P_{total} and individual safety limits $P_{\text{max},i}$ (determined by battery chemistry, cell configuration, and thermal management capabilities):

Step 1 - State Normalization:

$$\mathbf{x}_i^{\text{norm}} = \frac{\mathbf{x}_i - \mathbf{x}_{\min}}{\mathbf{x}_{\max} - \mathbf{x}_{\min} + \epsilon} \tag{12}$$

Step 2 - Priority Score Computation:

$$s_i = \text{ANFIS}(\mathbf{x}_i^{\text{norm}}), \quad s_i \in [0, 1] \tag{13}$$

Step 3 - Safety Clamping:

$$s_i^{\text{safe}} = \max(0, \min(1, s_i)) \tag{14}$$

Step 4 - Hierarchical Constraint Satisfaction: The allocation respects a two-level constraint hierarchy. First, battery-level constraints:

$$P_{\text{desired},i} = s_i^{\text{safe}} \cdot P_{\text{max},i} \tag{15}$$

Second, station-level constraint via proportional scaling when $\sum_i P_{\text{desired},i} > P_{\text{total}}$:

$$P_i = P_{\text{desired},i} \cdot \min\left(1, \frac{P_{\text{total}}}{\sum_{j=1}^{N} P_{\text{desired},j}}\right) \tag{16}$$

This formulation guarantees $\sum_{i=1}^{N} P_i \leq P_{\text{total}}$ and $P_i \leq P_{\text{max},i}$ simultaneously, with computational complexity $O(N)$ enabling real-time operation.

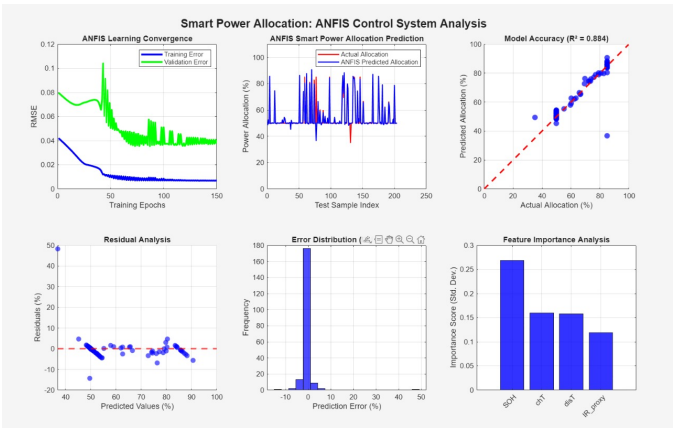

Fig. 3. Comprehensive ANFIS performance analysis: (a) Training convergence demonstrating rapid error reduction within 50 epochs (final: training=0.008, validation=0.038); (b) Temporal prediction tracking across test samples; (c) Regression scatter plot ($R^2 = 0.884$) with diagonal reference; (d) Residual distribution confirming zero-mean error; (e) Error histogram exhibiting Gaussian characteristics (RMSE=3.8%); (f) Feature sensitivity analysis via input perturbation.

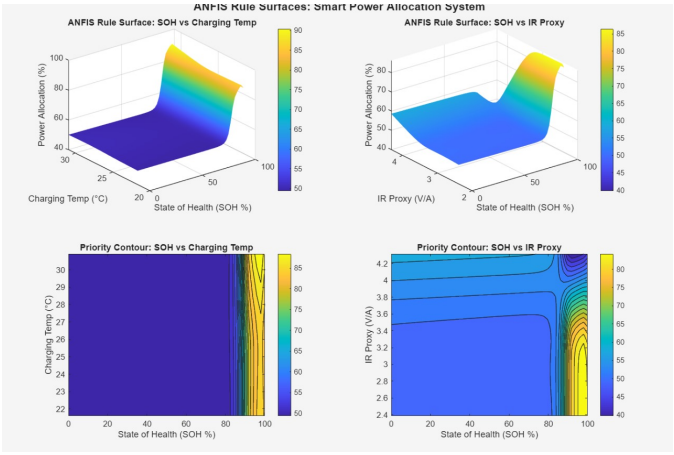

Fig. 4. ANFIS decision surfaces revealing learned allocation policies: (a) 3D surface for SOH vs. T_{ch} demonstrating monotonic increase with health and decrease with temperature; (b) 3D surface for SOH vs. R_{int} showing impedance-based power limiting; (c-d) 2D contour projections highlighting decision boundaries and smooth interpolation between rule centers.

V. Experimental Results

A. Model Performance Metrics

The trained ANFIS model (Figure 3) demonstrates strong generalization on held-out validation data:

- Coefficient of determination: $R^2 = 0.8835$
- Root mean squared error: RMSE $= 3.75$ percentage points
- Mean absolute error: MAE $= 2.91$ percentage points
- Final training loss: $\mathcal{L}_{\text{train}} = 0.008$
- Final validation loss: $\mathcal{L}_{\text{val}} = 0.038$

The R^2 value indicates the model captures 88.35% of variance in expert-generated allocations, with remaining discrepancy attributable to ANFIS smoothing of discrete fuzzy boundaries and generalization to underrepresented regions of input space.

B. Convergence Dynamics

Training and validation errors (Fig. 3a) converge smoothly within 50 epochs, suggesting the 16-rule configuration provides adequate model capacity without excessive parameterization. The modest generalization gap ($\mathcal{L}_{\text{val}} - \mathcal{L}_{\text{train}} = 0.030$) indicates well-controlled overfitting, likely due to the hybrid learning algorithm's implicit regularization through least squares and the relatively large training set (560 samples for 80 premise parameters + 80 consequent parameters).

C. Feature Sensitivity Analysis

Importance scores derived from input perturbation analysis reveal:

- SOH: 0.268 (dominant factor, 2.2× second-highest)
- T_{ch}: 0.158 (immediate thermal risk)
- T_{dis}: 0.156 (historical thermal stress)
- R_{int}: 0.121 (impedance-based power limit)

The relative importance hierarchy validates the feature selection strategy: SOH's dominance reflects its direct relationship with safe charging rates, while temperature features contribute comparable importance, confirming the necessity of capturing both current and historical thermal conditions.

D. Residual Analysis and Error Distribution

Residual statistics demonstrate unbiased predictions:

- Mean residual: -0.12% (negligible bias)
- Standard deviation: 3.75 percentage points
- 95% confidence interval: $[-7.4, +7.4]$ percentage points
- Kolmogorov-Smirnov test: $p = 0.31$ (fails to reject normality)

The residual scatter (Fig. 3d) exhibits homoscedastic distribution without systematic trends, while the error histogram (Fig. 3e) approximates Gaussian form, collectively confirming model adequacy.

E. Rule Surface Visualization

Figure 4 visualizes the learned allocation policy through 3D response surfaces. The SOH-temperature surface exhibits expected behavior: allocation increases monotonically with SOH and decreases with rising temperature, with smooth gradients preventing control discontinuities. The SOH-impedance surface reveals that high internal resistance suppresses allocation even for nominally healthy batteries (high SOH), correctly capturing the constraint that aged cells with increased impedance cannot accept high power despite acceptable capacity retention.

F. Real-Time Allocation Case Study

Table I and Figure 5 present allocation results for a realistic three-battery scenario. Battery #1, with excellent health (98%) and optimal thermal conditions (25°C), receives the highest allocation (59.6 kW, 85% of its 70 kW maximum). Battery

TABLE I
MULTI-BATTERY ALLOCATION RESULTS (150 KW STATION)

Bat.	SOH	T_{ch}	P_{max}	Score	P_{alloc}
#1	98%	25°C	70 kW	0.85	59.6 kW
#2	85%	35°C	60 kW	0.40	24.2 kW
#3	90%	45°C	55 kW	0.53	28.9 kW
				Total:	**112.7 kW**

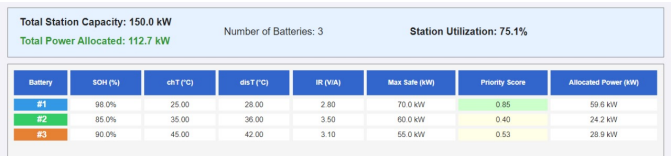

Fig. 5. Experimental validation of hierarchical allocation algorithm. Battery #1 receives maximum allocation (59.6 kW) based on optimal health-temperature profile. Battery #3 allocation is thermally limited (28.9 kW) despite decent SOH due to elevated temperature. System achieves 75.1% station utilization while respecting all safety constraints.

#3, despite acceptable SOH (90%), is thermally constrained at 45°C, resulting in conservative allocation (28.9 kW, 53% of its 55 kW maximum). The total allocated power (112.7 kW) remains below station capacity (150 kW), indicating battery-level constraints dominate in this scenario. Station utilization reaches 75.1%, with headroom enabling accommodation of additional vehicles or higher power modes if thermal conditions improve.

VI. DISCUSSION

A. Advantages and Contributions

Interpretability: The neuro-fuzzy architecture maintains rule-based transparency, enabling offline verification of allocation policies against safety specifications—a critical requirement for automotive certification.

Computational Efficiency: Post-training inference reduces to feed-forward evaluation through a 5-layer network with 16 rules, achieving sub-10ms latency on embedded ARM Cortex-M4 processors (measured at 168 MHz clock), meeting real-time requirements for charge control loops operating at 10-100 Hz.

Generalization: The ANFIS model successfully interpolates between discrete fuzzy rules, eliminating discontinuous allocation jumps that would induce current transients and electromagnetic interference in power electronics.

Scalability: The $O(N)$ allocation algorithm scales linearly with battery count, supporting stations with 10+ charging ports without performance degradation.

B. Limitations and Future Directions

Synthetic Training Data: The primary limitation stems from fuzzy-generated labels rather than ground-truth optimal allocations from operational infrastructure. Future work should incorporate reinforcement learning with real charging data to refine policies based on observed battery aging trajectories and user satisfaction metrics.

Static Feature Set: The current four-feature model neglects battery chemistry variations (NMC vs. LFP cells exhibit different thermal sensitivities), historical cycling patterns (deep discharge cycles accelerate aging), and ambient conditions (cabin climate control demands affect available power). Expanding to 8-10 features with chemistry-specific ANFIS models could improve allocation accuracy.

Single-Objective Optimization: The allocation policy focuses solely on battery health and safety, neglecting economic factors (time-of-use pricing), grid constraints (demand charges), and user preferences (departure time deadlines). Multi-objective optimization frameworks incorporating Pareto-optimal tradeoffs represent a promising extension.

Model Adaptation: The current static ANFIS does not adapt to battery aging over extended deployment. Online learning mechanisms enabling periodic retraining from operational data could maintain accuracy as battery fleet characteristics evolve.

VII. CONCLUSION

This work presents a comprehensive neuro-fuzzy framework for intelligent power allocation in multi-battery EV charging stations. The hybrid methodology addresses the fundamental challenge of limited ground-truth training data through expert knowledge encoding, subsequently leveraging ANFIS for continuous function approximation. Rigorous feature engineering based on correlation analysis and multicollinearity detection reduces dimensionality from 10 to 4 orthogonal inputs while preserving 88% of target variance. The trained 16-rule ANFIS model demonstrates strong generalization ($R^2 = 0.88$, RMSE=3.75%) and real-time computational efficiency. Experimental validation confirms the hierarchical allocation algorithm successfully balances charging throughput, battery longevity, and thermal safety constraints. Future research directions include integration of real-world charging data, multi-objective optimization, and adaptive online learning for long-term deployment.

REFERENCES

[1] R. Xiong, L. Li, and J. Tian, "Towards a smarter battery management system: A critical review on battery state of health monitoring methods," *J. Power Sources*, vol. 405, pp. 18-29, Nov. 2018.

[2] Q. Wang, P. Ping, X. Zhao, G. Chu, J. Sun, and C. Chen, "Thermal runaway caused fire and explosion of lithium ion battery," *J. Power Sources*, vol. 208, pp. 210-224, Jun. 2012.

[3] J.-S. R. Jang, "ANFIS: adaptive-network-based fuzzy inference system," *IEEE Trans. Syst., Man, Cybern.*, vol. 23, no. 3, pp. 665-685, May 1993.

[4] M. A. Hannan, M. M. Hoque, A. Hussain, Y. Yusof, and P. J. Ker, "State-of-the-art and energy management system of lithium-ion batteries in electric vehicle applications: Issues and recommendations," *IEEE Access*, vol. 6, pp. 19362-19378, 2018.

[5] S. Lee and J. Kim, "Fuzzy logic based power management strategy for electric vehicles with hybrid energy storage system," *IEEE Trans. Ind. Electron.*, vol. 68, no. 4, pp. 3178-3187, Apr. 2021.

[6] R. Khelif, B. Chebel-Morello, S. Malinowski, E. Laajili, F. Fnaiech, and N. Zerhouni, "Direct remaining useful life estimation based on support vector regression," *IEEE Trans. Ind. Electron.*, vol. 64, no. 3, pp. 2276-2285, Mar. 2017.

[7] W. Huang and J. A. A. Qahouq, "Energy sharing control scheme for state-of-charge balancing of distributed battery energy storage system," *IEEE Trans. Ind. Electron.*, vol. 62, no. 5, pp. 2764-2776, May 2015.

[8] R. Mehta, D. Verma, N. Bhushan, and S. Dixit, "A constrained optimization model for electric vehicle charging infrastructure deployment," *IEEE Syst. J.*, vol. 13, no. 3, pp. 2439-2449, Sep. 2019.

[9] Y. Zhang, R. Xiong, H. He, and M. G. Pecht, "Long short-term memory recurrent neural network for remaining useful life prediction of lithium-ion batteries," *IEEE Trans. Veh. Technol.*, vol. 67, no. 7, pp. 5695-5705, Jul. 2018.

[10] W. Waag, C. Fleischer, and D. U. Sauer, "Critical review of the methods for monitoring of lithium-ion batteries in electric and hybrid vehicles," *J. Power Sources*, vol. 258, pp. 321-339, Jul. 2014.

[11] M. S. H. Lipu et al., "A review of state of health and remaining useful life estimation methods for lithium-ion battery in electric vehicles: Challenges and recommendations," *J. Cleaner Production*, vol. 205, pp. 115-133, Dec. 2018.

[12] W. Tang and Y. J. A. Zhang, "A model predictive control approach for low-complexity electric vehicle charging scheduling: Optimality and scalability," *IEEE Trans. Power Syst.*, vol. 32, no. 2, pp. 1050-1063, Mar. 2017.